

The structure of radiative shock waves

IV. Effects of electron thermal conduction

Yu.A. Fadeyev¹, H. Le Coroller², and D. Gillet²

¹ Institute for Astronomy of the Russian Academy of Sciences, Pyatnitskaya 48, 109017 Moscow, Russia

² Observatoire de Haute-Provence - CNRS, F-04870 Saint-Michel l'Observatoire, France

Received September 2001 / Accepted

Abstract. We consider the structure of steady-state radiative shock waves propagating in the partially ionized hydrogen gas with density $\rho_1 = 10^{-10}$ gm cm⁻³ and temperature $3000 \text{ K} \leq T_1 \leq 8000 \text{ K}$. The radiative shock wave models with electron thermal conduction in the vicinity of the viscous jump are compared with pure radiative models. The threshold shock wave velocity above of which effects of electron thermal conduction become perceptible is found to be of $U_1^* \approx 70 \text{ km s}^{-1}$ and corresponds to the upstream Mach numbers from $M_1 \approx 6$ at $T_1 = 8000 \text{ K}$ to $M_1 \approx 11$ at $T_1 = 3000 \text{ K}$. In shocks with efficient electron heat conduction more than a half of hydrogen atoms is ionized in the radiative precursor, whereas behind the viscous jump the hydrogen gas undergoes the full ionization. The existence of the electron heat conduction precursor leads to the enhancement of the Lyman continuum flux trapped in the surroundings of the discontinuous jump. As a result, the partially ionized hydrogen gas of the radiative precursor undergoes an additional ionization ($\delta x_{\text{H}} \lesssim 5\%$), whereas the total radiative flux emerging from the shock wave increases by $10\% \leq \delta(F_{\text{R}}) \leq 25\%$ for $70 \text{ km s}^{-1} \leq U_1 \leq 85 \text{ km s}^{-1}$.

Key words. Shock waves – Hydrodynamics – Radiative transfer – Stellar atmospheres

1. Introduction

In our previous papers (Fadeyev & Gillet, 1998, 2000, 2001), hereinafter referred to as Papers I – III, we presented the studies of steady-state radiative shock waves propagating in the partially ionized hydrogen gas with properties that are typical for atmospheres of pulsating late-type stars. The models were considered in terms of the self-consistent solution of the equations of fluid dynamics, radiation transfer and rate equations for the hydrogen atom and provide the reliable estimates of radiative energy losses of the shock wave. In these studies we adopted that at the viscous jump which is treated as an infinitesimally thin discontinuity the electron gas compresses adiabatically. Such an assumption is justified by the very low rate of energy exchange between protons and electrons within the viscous jump and thereby allows us to determine the postshock electron temperature from the simple adiabatic relation. However, it is known that the characteristic length scale of electron thermal conduction might be comparable with the thickness of the postshock relaxation zone (the length of the temperature equilibration zone) and, therefore, might affect perceptibly the spatial distribution of hydrodynamic variables at least in the

vicinity of the viscous jump (see, for discussion, Zel'dovich & Raizer, 1967; Mihalas & Weibel Mihalas, 1984).

Effects of electron thermal conduction in two-temperature shock waves propagating in partially ionized helium and argon with temperatures and densities close to those of stellar atmospheres were investigated using both hydrodynamic and kinetic approaches by Grewal & Talbot (1963); Jaffrin (1965); Lu & Huang (1974). Solution of the more general problem involving the radiation transfer was considered by Vinolo & Clarke (1973). The conspicuous result of these calculations is that the authors demonstrated the existence of the zone of the elevated electron temperature ahead the viscous jump appearing due to the high thermal conductivity of the electron gas. For the hydrogen gas effects of electron thermal conduction were considered only in the limit of full ionization at Mach numbers as high as $M_1 \approx 8$ (Vidal et al., 1993, 1995). This study, unfortunately, was confined to the problem of inertial confinement fusion for the extremely high temperature and number density of electrons ($T = 10^8 \text{ K}$, $n_e = 10^{22} \text{ cm}^{-3}$).

By now, the scarce studies of astrophysical radiative shock waves with electron thermal conduction in two-temperature gases were confined to the interstellar medium (Borkowski et al., 1989; Borkowski & Shull, 1990) and accreting white dwarfs (Imamura et al., 1987). In these works the heat conduction was found to substan-

tially affect the structure of the postshock relaxation zone for shocks with velocities ranged from 70 km s⁻¹ to 170 km s⁻¹. In atmospheres of late-type pulsating stars the gas density is many orders of magnitude higher in comparison with that of the interstellar medium, whereas the velocities of shocks does not exceed 100 km s⁻¹, so that the role of electron heat conduction in radiative losses remains highly uncertain. In this paper we compute the models of steady-state radiative shock waves propagating through the partially ionized hydrogen gas with properties typical for atmospheres of pulsating late-type stars and compare the pure radiative shock wave models with those in which electron the thermal conduction is taken into account.

As in our previous papers we assume that the ambient unperturbed medium is homogeneous and effects of magnetic fields are negligible. Indeed, the magnetic field becomes important when the electron mean free path l_e is larger than the gyromagnetic radius r_B . For the gas density considered in our study ($\rho = 10^{-10}$ gm cm⁻³) the condition $l_e \gg r_B$ fulfills for $B \gg 3$ Gauss. Furthermore, the magnetic pressure $B^2/8\pi$ becomes comparable with the gas pressure for $B > 25$ Gauss. On the other hand, the strength of the magnetic field in late-type giants is $B \ll 1$ Gauss (Belvedere et al., 1982). Thus, effects of magnetic fields can be ignored without any loss of accuracy. We expect that results of our calculations can be applied to shock phenomena observed in atmospheres of radially pulsating giants and supergiants such as W Vir, RV Tau and Mira type variables.

In order to specify the model we use three parameters determining the structure of the steady-state radiative shock wave. These are the density ρ_1 and the temperature T_1 of the ambient hydrogen gas and the upstream gas flow velocity U_1 .

2. Equations for thermal conduction

Detailed discussion of the basic equations used for calculation of the structure of radiative shock waves is given in our earlier papers and in this section we only consider the equations involving the terms responsible for electron thermal conduction. Eq. (20) of Paper II describes the change of the translational specific energy of the electron gas

$$\tilde{E}_e = \frac{3}{2} \frac{n_e}{\rho} kT_e \quad (1)$$

and is written now as

$$\begin{aligned} \frac{d\tilde{E}_e}{dt} = & - P_e \frac{dV}{dt} + Q_{\text{elc}} - \frac{d\tilde{E}_I}{dt} - \frac{d\tilde{E}_{\text{ex}}}{dt} - \frac{1}{\rho} \frac{dE_R}{dt} - \\ & - \frac{1}{\rho} \nabla \cdot \mathbf{F}_R - \frac{1}{\rho} \nabla \cdot \mathbf{F}_e. \end{aligned} \quad (2)$$

Here n_e is the number density of free electrons, $P_e = n_e kT_e$ is the partial pressure of the electron gas, $V = 1/\rho$ is the specific volume, Q_{elc} is the rate of energy gain by electrons in elastic collisions with neutral hydrogen atoms

and hydrogen ions, \tilde{E}_I and \tilde{E}_{ex} are the ionization energy and the excitation energy per unit mass, E_R and \mathbf{F}_R are the radiation energy density and the total radiation flux, respectively,

$$\mathbf{F}_e = -\mathcal{K}_e \nabla T_e \quad (3)$$

is the electron heat conductive flux. The thermal conductivity \mathcal{K}_e was calculated using the fitting formulae (Nowak & Ulmschneider, 1977) taking into account effects of partial ionization and converging with those given by Spitzer (1962) for the fully ionized hydrogen.

Equation (3) is valid until the mean free path of electrons is smaller than the characteristic temperature scale and for the too steep temperature gradient it becomes inapplicable due to effects of saturation of the heat flux. According to Cowie & McKee (1977) the saturated heat flux q_{sat} is proportional to the product of the thermal energy of electrons and their mean thermal velocity, that is,

$$q_{\text{sat}} = f \left(\frac{2kT_e}{\pi m_e} \right)^{1/2} n_e kT_e. \quad (4)$$

Unfortunately, the value of the flux limit factor f for the partially ionized hydrogen gas is uncertain. Cowie & McKee (1977) adopted $f = 0.4$, whereas Borkowski et al. (1989) presented arguments in favour of $f \sim 0.1$. According to more recent kinetic calculations (Vidal et al., 1995) the flux limit factor is $f \approx 0.3$ and it is the value that we used in our study.

The presence of the divergence of the conductive flux in Eq. (2) increases the order of this equation and leads to the much stronger sensitivity of the resulting system of ordinary differential equations (see Eqs. (17) – (21) of Paper II) to the round-off errors. To keep the first order of Eq. (2) we calculated $\nabla \cdot \mathbf{F}_e$ each iteration together with solution of the radiation transfer equation for the given spatial distribution of hydrodynamic variables. For the first iteration we replaced the spatial distribution of the electron temperature T_e obtained from the pure radiative model and having the jump at the discontinuity by the arbitrary function smoothing the run of T_e within ~ 100 cm in both sides of the discontinuous jump. After the series of trial calculations we found that the final solution does not depend on the initial distribution of T_e since the region of the effective energy transfer by electron thermal conduction is by an order of magnitude narrower. The shock wave models were represented by $2000 \leq N \leq 8000$ cells with $\sim 10^3$ cells within the thermal conduction region.

The divergence of the conductive flux was computed using the second-order finite-difference formula

$$\begin{aligned} (\nabla \cdot \mathbf{F}_e)_{j-1/2} = & - \frac{\mathcal{K}_{e,j-1}}{\Delta X_{j-1}} \frac{T_{e,j-3/2}}{\Delta X_{j-1/2}} + \\ & + \left(\frac{\mathcal{K}_{e,j-1}}{\Delta X_{j-1}} + \frac{\mathcal{K}_{e,j}}{\Delta X_j} \right) \frac{T_{e,j-1/2}}{\Delta X_{j-1/2}} - \frac{\mathcal{K}_{e,j}}{\Delta X_j} \frac{T_{e,j+1/2}}{\Delta X_{j-1/2}}, \end{aligned} \quad (5)$$

where $\Delta X_j = \frac{1}{2}(\Delta X_{j-1/2} + \Delta X_{j+1/2})$ and $\Delta X_{j-1/2} = X_j - X_{j-1}$ are the space intervals. All thermodynamic quantities are defined at cell centers having half-integer subscripts and the conductivity coefficient at cell interfaces is determined as the mass-weighted average:

$$\mathcal{K}_{e_j} = \frac{\mathcal{K}_{e_{j-1/2}}\Delta m_{j-1/2} + \mathcal{K}_{e_{j+1/2}}\Delta m_{j+1/2}}{\Delta m_{j-1/2} + \Delta m_{j+1/2}}, \quad (6)$$

where $\Delta m_{j-1/2} = \rho_{j-1/2}\Delta X_{j-1/2}$ is the mass contained in the cell $[X_{j-1}, X_j]$. Thus, the divergence of the conductive flux in Eq. (2) was considered explicitly and during integration of the ordinary differential equations was calculated using the nonlinear interpolation.

The discontinuity is assumed to locate at the j -th cell interface with space coordinate $X_j = 0$, so that coordinates of cell centers just ahead and just behind the discontinuity are $X_{j-1/2}$ and $X_{j+1/2}$. For the sake of convenience the quantities defined at these cell centers are denoted by superscripts minus and plus, respectively. In all models considered in our study the size of the central cell was set equal to $\Delta X_j = X_{j+1/2} - X_{j-1/2} = 0.1$ cm.

Solution of the preshock initial-value problem is ended at the $(j - 1/2)$ -th cell center and in order to obtain the initial conditions for the postshock integration we use the Rankine–Hugoniot equations relating quantities at both sides of the discontinuity at cell centers $X_{j-1/2}$ and $X_{j+1/2}$. For the radiative shock wave with electron heat conduction the Rankine–Hugoniot equations are written as

$$\rho U = \mathcal{C}_0 \equiv \dot{m}, \quad (7)$$

$$\dot{m}U + P_g + P_R = \mathcal{C}_1, \quad (8)$$

$$\frac{1}{2}\dot{m}U^2 + \dot{m}h + F_e + F_R + U(E_R + P_R) = \mathcal{C}_2, \quad (9)$$

where h is the specific enthalpy (see Eq. (7) of Paper II), P_g is the gas pressure, P_R is the radiation pressure, \mathcal{C}_0 , \mathcal{C}_1 and \mathcal{C}_2 are the mass, momentum and energy fluxes. Solution of the Rankine–Hugoniot relations gives the compression ratio across the discontinuous jump $\eta = \rho^+/\rho^-$ as the root of the quadratic equation

$$A\eta^2 - B\eta + C = 0, \quad (10)$$

where

$$A = (a_T^-)^2 + \frac{1}{5}(U^-)^2 - \frac{2}{5}\frac{F_e^+ + F_R^+ - F_e^- - F_R^-}{\dot{m}} + \frac{2}{5}\frac{E_R^- + P_R^-}{\rho^-}, \quad (11)$$

$$B = (a_T^-)^2 + (U^-)^2 + \frac{2}{5}\frac{E_R^+ + P_R^+}{\rho^-} - \frac{P_R^+ - P_R^-}{\rho^-}, \quad (12)$$

$$C = \frac{4}{5}(U^-)^2, \quad (13)$$

$a_T = (P_g/\rho)^{1/2}$ is the isothermal sound speed.

In contrast to our earlier studies where we assumed that the electron gas compresses at the viscous jump adi-

abatically in the present paper we employed the jump condition for the electron temperature written as

$$T_e^+ = T_e^- - \frac{F_{e_j}}{\mathcal{K}_{e_j}}\Delta X_j. \quad (14)$$

The postshock temperature of heavy particles is obtained from solution of Eqs. (7–9) and is given by

$$T_a^+ = T_a^- - \frac{n_e^-}{n_H}(T_e^+ - T_e^-) + \frac{1}{5}\frac{\dot{m}U^-}{n_H k}\frac{\eta^2 - 1}{\eta^2} - \frac{2}{5}\frac{F_e^+ + F_R^+ - F_e^- - F_R^-}{n_H k U^-} - \frac{2}{5}\frac{(E_R^+ + P_R^+)\eta^{-1} - (E_R^- + P_R^-)}{n_H k}, \quad (15)$$

where n_H is the number density of hydrogen atoms.

3. The structure of shocks with heat conduction

In solution of the initial-value problem for the fluid dynamics and rate equations we considered the system of ordinary differential equations described in Paper II. The only exception is that within the interval $X_{ca} = -100$ cm $\leq X \leq X_{cb} = 100$ cm surrounding the discontinuous jump the equation for E_e (Eq. (20) of Paper II) is replaced by Eq. (2). The large size of the interval with heat conduction taken into account was used in order to diminish the role of boundary conditions $F_e(X_{ca}) = F_e(X_{cb}) = 0$ in calculations of the divergence of conductive flux $\nabla \cdot \mathbf{F}_e$.

The vicinity of the discontinuous jump of the shock wave model with $\rho_1 = 10^{-10}$ gm cm $^{-3}$, $T_1 = 3000$ K and $U_1 = 75$ km s $^{-1}$ is shown in Fig. 1 where as a function of X are plotted the electron temperature T_e and the temperature of heavy particles T_a (upper panel), the heat conductive flux F_e , the Lyman continuum flux F_{Ly} and the saturated heat flux q_{sat} (middle panel), the divergence of the heat conductive flux $\nabla \cdot \mathbf{F}_e$ and the divergence of the total radiative flux $\nabla \cdot \mathbf{F}_R$ (lower panel). It should be noted that in the framework of our model the space coordinate X increases while the gas element passes through the shock wave and in such a notation the upstream and downstream fluxes are negative and positive, respectively.

In the unperturbed hydrogen gas with density $\rho_1 = 10^{-10}$ gm cm $^{-3}$ and the temperature of 3000 K $\leq T_1 \leq 6000$ K the length of the radiative precursor is $\sim 10^4$ cm and at the upstream gas flow velocity $U_1 = 75$ km s $^{-1}$ the temperature growth due to absorption of the Lyman continuum radiation emerging from the postshock region is $(\Delta T)_r \approx 2000$ K. As is seen from Fig. 1 the length of the region of efficient heat conduction surrounding the discontinuous jump is of ~ 10 cm. Within such a narrow interval the divergence of the heat conductive flux exceeds the divergence of radiative flux by almost two orders of magnitude, so that the heating and cooling of gas are due to the electron heat conduction and the role of radiation is negligible.

For the model represented in Fig. 1 the electron temperature growth within the conductive precursor is of

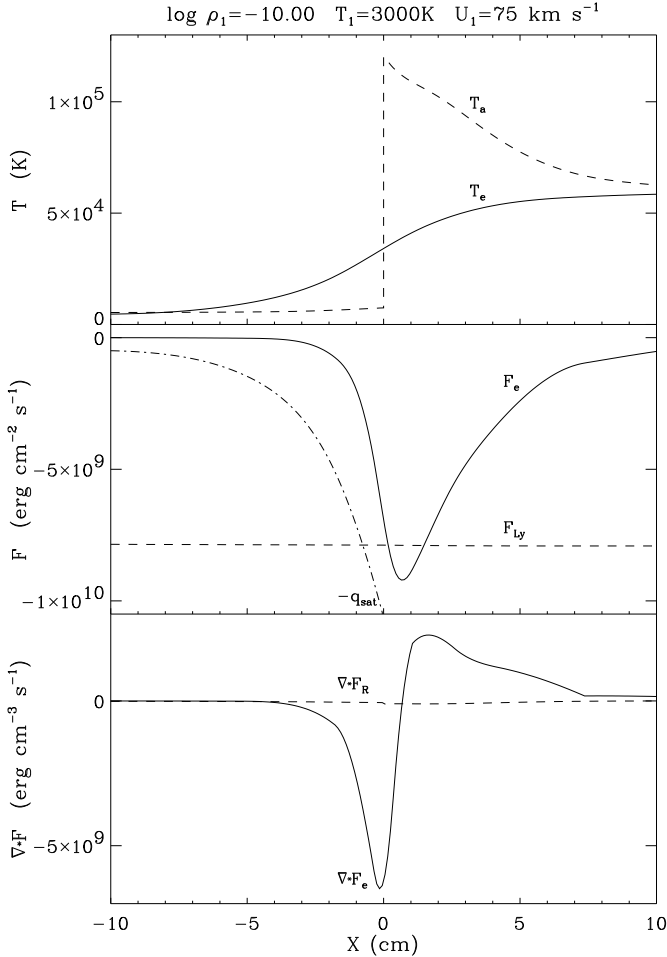


Fig. 1. The vicinity of the discontinuous jump located at $X = 0$ of the shock wave model with $\rho_1 = 10^{-10} \text{ gm cm}^{-3}$, $T_1 = 3000 \text{ K}$ and $U_1 = 75 \text{ km s}^{-1}$. Upper panel: the electron temperature T_e (solid line) and the temperature of heavy particles T_a (dashed line). Middle panel: the heat conductive flux F_e (solid line), the Lyman continuum flux F_{Ly} (dashed line) and the saturated heat flux q_{sat} (dot-dashed line). Lower panel: the divergence of the heat conductive flux $\nabla \cdot \mathbf{F}_e$ (solid line) and the divergence of the total radiative flux $\nabla \cdot \mathbf{F}_R$ (dashed line).

$(\Delta T_e)_c \approx 3 \cdot 10^4 \text{ K}$. A small fraction of the translational energy of the electron gas is lost in elastic collisions with hydrogen ions and the temperature of heavy particles increases within the conductive precursor by $(\Delta T_a)_c \approx 2000 \text{ K}$.

The heat conductive flux F_e does not exceed the total radiative flux and its maximum value is only comparable with the Lyman flux F_{Ly} (see the middle panel of Fig. 1) which is of ≈ 40 percent of the total radiative flux F_R . As is seen from Fig. 1 effects of saturation can play perceptible role only in the conductive precursor just ahead the discontinuous jump, whereas behind the discontinuity $q_{sat} \gg |F_e|$ because of higher density and higher temperature of the gas.

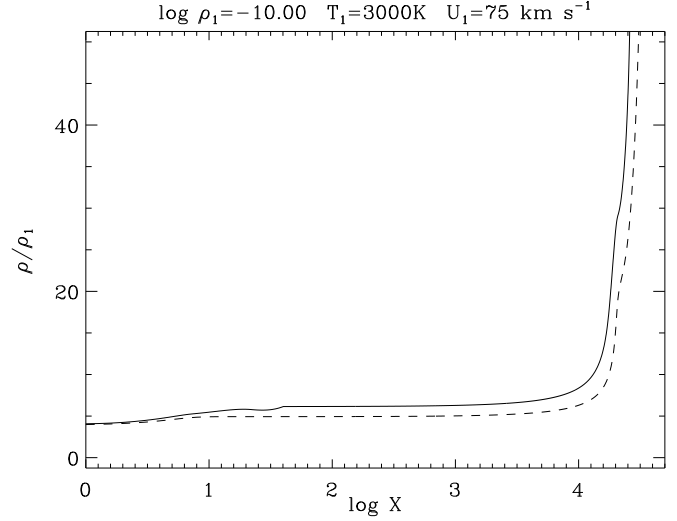


Fig. 2. The postshock compression ratio ρ/ρ_1 in the shock wave model with electron heat conduction (solid line) and in the pure radiative model (dashed line).

The growth of the preshock electron temperature due to conductive heating is accompanied by increase of the gas density. For example, in the pure radiative model with $\rho_1 = 10^{-10} \text{ gm cm}^{-3}$, $T_1 = 3000 \text{ K}$ and $U_1 = 75 \text{ km s}^{-1}$ the preshock compression ratio is $(\rho^-/\rho_1)_r = 1.008$, whereas in the model with heat conduction the preshock compression ratio is $(\rho^-/\rho_1)_c = 1.04$. The difference in compression ratios becomes more significant in the postshock region and increases with increasing distance from the discontinuous jump. For example, at the boundary of the thermalization zone ($\log X \approx 1$) the ratio of gas densities evaluated for the conductive and pure radiative models is $\rho_c/\rho_r \approx 1.1$, whereas at the boundary of the recombination zone ($\log X \approx 4.5$) this ratio is as high as $\rho_c/\rho_r \approx 1.6$. Two plots of the postshock compression ratios ρ/ρ_1 for the conductive and radiative shock wave models are shown in Fig. 2.

The stronger compression in shock waves with heat conduction implies that relaxation processes are somewhat faster in comparison with those in pure radiative shocks. Such a difference is due to the fact that existence of the preshock conductive precursor leads to the elevation of the radiation energy density within the whole area of the trapped Lyman continuum radiation. This area is confined by the layers of hydrogen ionization in the preshock region (the radiative precursor) and by the layers of hydrogen recombination behind the discontinuous jump. The enhancement of the radiation energy density is illustrated in Fig. 3 where we plot the Lyman continuum flux as a function of X for pure radiative and for the conductive model. For the sake of convenience we use the logarithmic scales for the both preshock and postshock regions that are represented by the left and by the right panels, respectively.

As was shown in our earlier papers (see, for example, Paper I and Paper II) the populations of atomic levels are governed by radiative transitions because the rates

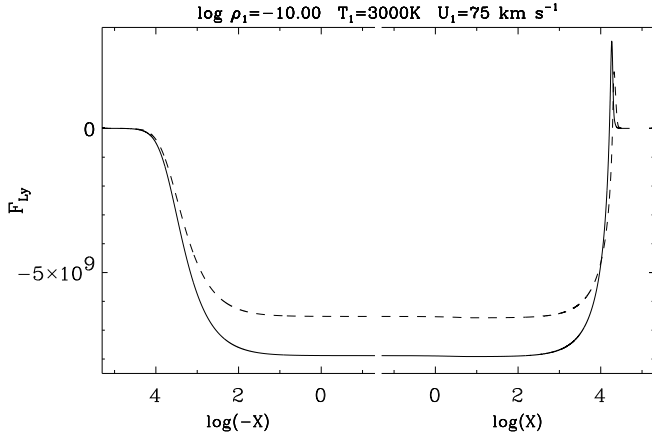


Fig. 3. The Lyman continuum flux in the conductive (solid line) and pure radiative (dashed line) shock waves. The left and the right panels represent the preshock and postshock regions, respectively.

of corresponding collisional transitions are several orders of magnitude smaller throughout the whole shock wave. Thus, elevation of the radiation energy density in the Lyman continuum leads to the larger preshock hydrogen ionization degree and at the same time to the faster ionization (if the hydrogen gas is still partially ionized in the radiative precursor) in the postshock region. This effect is illustrated in Fig. 4 representing the spatial distributions of the electron temperature T_e and the hydrogen ionization degree x_H for the both conductive and pure radiative shock wave models.

The efficiency of electron heat conduction in radiative shock waves depends on the hydrogen ionization degree ahead the discontinuous jump as well as on the electron temperature behind the discontinuous jump. Obviously, both these quantities increase with increasing upstream gas flow velocity U_1 though the preshock hydrogen ionization degree depends also on the temperature T_1 of the unperturbed ambient gas. In order to determine the threshold upstream velocity U_1^* for electron thermal conduction we computed a number of models with different values of T_1 and U_1 but for the fixed value of the unperturbed gas density $\rho_1 = 10^{-10}$ gm cm $^{-3}$. Results of these computations are summarized in Table 1 where the columns headed by U_1 , T_1 and M_1 give the upstream gas flow velocity in km s $^{-1}$, the temperature of the unperturbed hydrogen gas and the upstream Mach number. The column headed by x_H^- gives the hydrogen ionization degree just ahead the discontinuous jump of the shock wave model with electron heat conduction and the column headed by $\delta(x_H^-)$ gives the raise of the preshock hydrogen ionization degree in comparison with the pure radiative model. We found that the preshock raise of the hydrogen ionization degree due to effects of the electron heat conduction is $\delta(x_H^-) \lesssim 0.05$. Obviously, $\delta(x_H^-) = 0$ not only in the weak shocks with negligible heat conduction but also in strong shocks with full ionization of the preshock hydrogen gas. In the latter case the excess of the radiation energy density

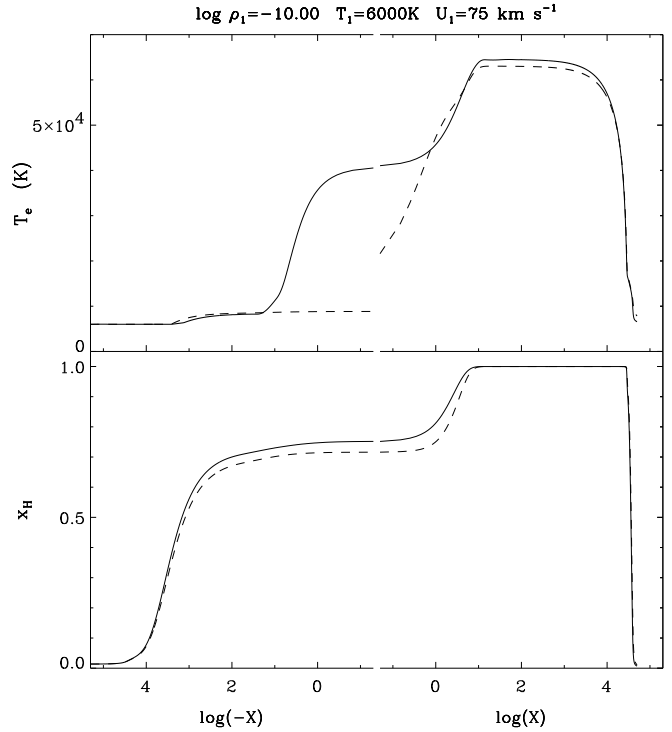


Fig. 4. The electron temperature T_e (upper panel) and the hydrogen ionization degree x_H (lower panel). In solid and dashed lines are represented the conductive and pure radiative models. The meaning of the left and the right panels is the same as in Fig. 3.

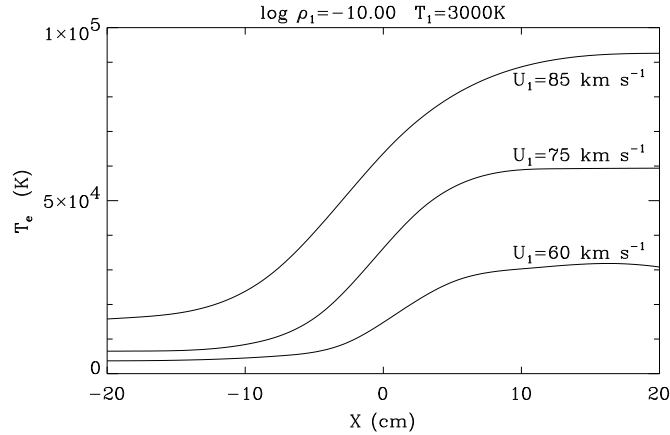
in the Lyman continuum leads to the stronger radiative heating of the preshock gas.

In order to evaluate the role of electron thermal conduction in the structure of radiative shock waves we compare the preshock gas density ρ^- , the Lyman continuum flux at the discontinuous jump $F_{Ly,\delta}$ and the total radiative flux emerging from the both boundaries of the shock wave model $F_R = \frac{1}{2}(F_{R,1} + F_{R,N})$ with corresponding quantities evaluated for the pure radiative models. To this end in last three columns of Table 1 we list the ratios $\varepsilon(\rho^-) = (\rho^-)_c/(\rho^-)_r$, $\varepsilon(F_{Ly,\delta}) = (F_{Ly,\delta})_c/(F_{Ly,\delta})_r$ and $\varepsilon(F_R) = (F_R)_c/(F_R)_r$.

As is seen from Table 1, the threshold upstream velocity is $U_1^* \approx 70$ km s $^{-1}$ and effects of electron thermal conduction become perceptible in strong shock waves with fully ionized hydrogen behind the discontinuous jump. At upstream gas flow velocities $U_1 \geq 70$ km s $^{-1}$ the postshock electron temperature is enough high in order to support the necessary temperature gradient and at the same time to ionize more than a half of hydrogen atoms in the radiative precursor by the strong Lyman continuum flux emerging from the postshock region. Shown in Fig. 5 plots of the electron temperature in the vicinity of the discontinuous jump illustrate a very rapid growth of the conductive precursor with increasing upstream velocity U_1 . Indeed, in the upstream velocity range 70 km s $^{-1} \leq U_1 \leq 85$ km s $^{-1}$ the additional radiative losses due to effects of electron

Table 1. Properties of radiative shock waves with electron heat conduction at $\rho_1 = 10^{-10}$ gm cm $^{-3}$.

U_1	T_1	M_1	x_{H}^-	$\delta(x_{\text{H}}^-)$	$\varepsilon(\rho^-)$	$\varepsilon(F_{\text{Ly},\beta})$	$\varepsilon(F_{\text{R}})$
65	8000	5.2	0.84	0.02	1.04	1.19	1.14
70	3000	10.9	0.47	0.01	1.02	1.08	1.03
	6000	7.7	0.73	0.02	1.05	1.21	1.16
	8000	5.6	1.	0.	1.08	1.30	1.28
75	3000	11.7	0.62	0.02	1.03	1.13	1.07
	6000	8.2	0.75	0.04	1.04	1.20	1.14
	8000	6.0	1.	0.	1.10	1.33	1.30
80	3000	12.5	0.86	0.05	1.09	1.38	1.32
	6000	8.8	0.98	0.01	1.06	1.25	1.20
	8000	6.4	1.	0.	1.08	1.27	1.26
85	3000	13.2	1.	0.	1.10	1.30	1.26

**Fig. 5.** The electron temperature T_e in the vicinity of the discontinuous jump in radiative shock waves with electron thermal conduction at upstream velocities $U_1 = 60, 75$ and 85 km s $^{-1}$.

heat conduction change from almost negligible values up to a quarter of the total radiative flux. Finally, as follows from Table 1, the higher temperature of the ambient gas significantly favours the electron heat conduction due to the higher ionization of the unperturbed ambient gas.

4. Conclusion

In this paper we have shown that in radiative shock waves with upstream velocities of $U_1 \gtrsim 70$ km s $^{-1}$ the physical properties of the gas surrounding the discontinuous jump are sufficient for appearance of efficient electron heat conduction, the conductive flux being comparable with the Lyman continuum flux in the vicinity of the discontinuous jump. The existence of the narrow conductive precursor affects all the region of the Lyman continuum radiation trapped around the discontinuous jump between zones of preshock ionization and postshock recombination of the hydrogen gas. As a consequence, the hydrogen ionization degree increases in the radiative precursor by as much as 5% provided that the preshock hydrogen gas is partially ionized. The effect of the saturation of the electron

conductive flux can be important only ahead the discontinuity but for models considered in the present study we obtained $|F_e| \lesssim q_{\text{sat}}$. The main conclusion of our study is that in shocks with velocities exceeding the threshold value $U_1^* \approx 70$ km s $^{-1}$ the electron thermal conduction significantly raises the radiative losses and, therefore, can diminish the efficiency of the shock-driven mass loss. More studies of radiative shock waves with electron heat conduction for wider ranges of ρ_1 , T_1 and U_1 are needed.

Acknowledgements. The work of YAF has been done in part under the auspices of the Ministère de la Recherche Française as well as was supported in part by the Russian National Program “Astronomy” (item 1102). This paper is a part of PhD of H. Le Coroller.

References

- Belvedere, G., Chiuderi, C., & Paterno, L. 1982, A&A, 105, 133
- Borkowski, K. J. & Shull, J. M. 1990, ApJ, 348, 169
- Borkowski, K. J., Shull, J. M., & McKee, C. F. 1989, ApJ, 336, 979
- Cowie, L. L. & McKee, C. F. 1977, ApJ, 211, 135
- Fadeyev, Y. A. 2001, Astronomy Reports, 45, 361
- Fadeyev, Y. A. & Gillet, D. 1998, A&A, 333, 687 (Paper I)
- . 2000, A&A, 354, 349 (Paper II)
- . 2001, A&A, 368, 901 (Paper III)
- Grewal, M. S. & Talbot, L. 1963, J. Fluid Mech., 16, 573
- Imamura, J. N., Durisen, R. H., Lamb, D. Q., & Weast, G. J. 1987, ApJ, 313, 298
- Jaffrin, M. Y. 1965, Phys.Fluids, 8, 606
- Lu, C. S. & Huang, A. B. 1974, Phys.Fluids, 17, 1527
- Mihalas, D. & Weibel Mihalas, B. 1984, Foundations of radiation hydrodynamics (New York: Oxford University Press, 1984)
- Nowak, T. & Ulmschneider, P. 1977, A&A, 60, 413
- Spitzer, L. 1962, Physics of Fully Ionized Gases (Physics of Fully Ionized Gases, New York: Interscience (2nd edition), 1962)
- Vidal, F., Matte, J. P., Casanova, M., & Larroche, O. 1993, Physics of Fluids B, 5, 3182
- . 1995, Physics of Plasmas, 2, 1412
- Vinolo, A. R. & Clarke, H. 1973, Phys.Fluids, 16, 1612
- Zel’dovich, Y. B. & Raizer, Y. P. 1967, Physics of shock waves and high-temperature hydrodynamic phenomena (New York: Academic Press, 1966/1967, edited by Hayes, W.D.; Probstein, Ronald F.)